Department of Physics and Astronomy
Heidelberg University

Bachelor thesis in Physics
submitted by

Junis Heiland Hoyo
born in Stuttgart, Germany

2023

Hadronic and Leptonic Vacuum Polarisation, Nuclear Structure and Hyperfine Structure in Highly Charged Ions

This Bachelor thesis has been carried out by
Junis Heiland Hoyo
at the
Max Planck Institute for Nuclear Physics
under the supervision of
PD Dr. Zoltán Harman

Zusammenfassung:

In dieser Arbeit wird die Hyperfeinstruktur von gebundenen Elektronen in wasserstoffartigen Ionen und die Korrekturen derer Energieniveaus durch quantenelektrodynamische (QED) Effekte betrachtet. Korrekturen zur Wellenfunktion sowie zum magnetischen Potential werden für leptonische und hadronische Vakuumpolarisation (VP) bestimmt. Die hadronische VP wird dabei semi-empirisch betrachtet. Eine numerische Methode für die Bestimmung der Verschiebung der Energieniveaus wird vorgestellt und die Ergebnisse werden mit Literaturwerten sowie mit bekannten Näherungsformeln verglichen. Unsicherheiten aufgrund des Kernradius werden angegeben und diskutiert. Es werden Punkt-, Kugel- und Fermi-Modelle für den Kern betrachtet und die Abweichung der Ergebnisse wird diskutiert.

Abstract:

In this thesis, the hyperfine structure of bound electrons in hydrogen-like ions is considered with corrections to the energy levels due to quantum electrodynamics (QED). Corrections to the wave function as well as the magnetic potential are determined for leptonic and hadronic vacuum polarisation (VP). Hadronic VP is treated with a semi-empirical approach. A numerical method to determine the energy shift is presented and the results are compared to values found in literature, as well as to known approximations. Uncertainties due to the nuclear radius are given and discussed. Point-like, spherical and Fermi distributed nuclear models are considered and the differences of the results are discussed.

Contents

1 Introduction

In 1926, Erwin Schrödinger introduced his equation, allowing a quantum mechanical description of probability waves. He derived the equation from the non-relativistic energy-momentum relation $E_{kin} = \frac{1}{2}mv^2$. Therefore, the energy in his equation was proportional to the momentum squared. However, even at the time it was known that, relativistically, the energy squared was actually proportional to the momentum squared

$$E^2 = m^2p^2 + m^2c^4, \tag{1.1}$$

which stood in direct disagreement with his equation. Two years later, in 1928, Paul Dirac then introduced the Dirac equation, accounting for relativistic effects by forcing linearity in all space-time coordinates [1]

$$\sqrt{\boldsymbol{p}^2c^2 + m^2c^4} \stackrel{!}{=} \boldsymbol{\alpha} \cdot \boldsymbol{p}\ c + \beta mc^2. \tag{1.2}$$

When considering the movement of an electron bound to a nucleus, especially as the nucleus increases in charge, and thus, size, relativistic effects are extremely relevant to consider and calculations have to be carried out accordingly.

These first formulations of a quantum theory evolved, finally resulting in the theory of quantum electrodynamics (QED). Nowadays, due to its almost unparalleled predictive accuracy, it is considered to be one of the most successful theories [2].

Introducing strong external fields, such as the one created by a heavy atomic nucleus, allows us to further test its validity in more extreme conditions. At the same time, high-precision experiments used to measure fundamental constants and to test them against theoretical values grow more accurate, giving rise to the need to calculate correction terms that have previously been considered negligible [3].

One of the best known atomic properties to be determined to very high accuracy in such a way is the g-factor. It describes the coupling of a particle with a magnetic moment to an external magnetic field. Following Dirac's relativistic theory, the value for the g-factor of a free electron was predicted to be 2. However, measurements in Ref. [4] showed that this was, in fact, not the case. The theoretical value only coincided with the findings when introducing corrections resulting from QED, granting the theory its popularity.

Contrary to the free electron, we can also consider bound electrons in strong nuclear fields. Here, the results also depend on the nucleus used, introducing an additional variable, and thus, more possibilities to test the theory. The simplest atomic model to consider is a hydrogen-like ion, where all electrons but one are stripped from the atom. Further, we can distinguish the nuclear model, with the

simplest approach being a point-like nucleus with no dimensions. When considering finite nuclear size (fns), we usually regard either a spherical model or the more accurate, but also computationally more demanding, Fermi distribution.

Another phenomenon not as commonly talked about is the hyperfine structure. It arises from atoms with nuclear spin and, therefore, generating a spherically symmetric magnetic field. The bound electron now interacts with that field instead of a homogeneous external magnetic field, which leads to a different shift in energy. Compared to the energy shift when considering the g-factor, fewer corrections to this shift, usually denoted by parameters ε, have been determined. However, given its comparatively smaller influence, it is of great interest since it, in turn, might also be more sensitive to effects previously disregarded, such as the nuclear model and, therefore, allows for more detailed tests of QED.

In this thesis, we will look at vacuum polarisation (VP), a specific QED correction, and how it changes the hyperfine splitting on an energy level of a bound electron.

The structure of this thesis is as follows. In chapter 2, a general description of bound electrons is given. We outline solutions to the Dirac equation for point-like, spherical and Fermi distributed nuclei. We also discuss how to perturbatively treat QED corrections as well as hyperfine structure to change the results obtained from the Dirac equation. In chapter 3, we discuss the calculations concerning vacuum polarisation corrections in more detail. We determine how the photon propagator is changed by this effect and how this leads to a perturbation of the Coulomb potential, also called the Uehling potential. We then outline how the specific expressions for the Uehling potential can be determined for leptonic and hadronic VP. For leptonic VP, we follow the analytical approach given in Ref. [5] and for hadronic VP, we follow the semi-empirical treatment discussed in Ref. [6] for both point-like and extended nuclei. In chapter 4, we discuss the numerical methods used to determine our results for extended nuclei. We introduce the concept of Bézier curves and B-splines, as well as a finite basis set, to describe the solutions to the Dirac equation. We then present how to implement B-splines to solve the radial Dirac equation. In chapter 5, we introduce the convention used to describe QED effects when considering hyperfine structure and discuss how the two effects can interact with each other. Finally, we present our results, compare them to values cited in literature, as well as previously known approximations, and give a brief outlook for future work.

In this thesis, we use natural units with the reduced Planck constant $\hbar$, the vacuum speed of light c and the vacuum permittivity ε_0 set to unity ($\hbar = c = \varepsilon_0 = 1$). In our final calculations we further set the mass of the electron to unity $m_e = 1$. The charge of the electron is defined by $e < 0$ and the fine-structure constant is given by $\alpha = e^2/(4\pi)$ in this system of units[1].

The inner product of two four-vectors a_μ and b_μ, using Einstein's summation convention, is given by $a_\mu b^\mu = a_0 b_0 - \boldsymbol{a} \cdot \boldsymbol{b}$.

[1] We use the most recent values from 2018 given by CODATA [7] (https://physics.nist.gov/cuu/Constants/index.html)

2 Description of bound electrons

In general, a good approximation to determine the energy level of a bound electron can be achieved by solving the stationary Schrödinger equation in the Coulomb potential of the nucleus

$$\left(\frac{\boldsymbol{p}}{2m_e} - \frac{Z\alpha}{r}\right)\psi_{nlm}(\boldsymbol{r}) = E_n\psi_{nlm}(\boldsymbol{r}), \tag{2.1}$$

where m_e denotes the mass of the electron, $\boldsymbol{p}$ the momentum operator, $\alpha = e^2/4\pi \approx 1/137$ the fine-structure constant defined through the electron charge e and Z the nuclear charge number such that $-Ze$ is the charge of the nucleus. ψ_{nlm} are the resulting wave functions and E_n the energy eigenvalues given by

$$E_n = -\frac{m_e}{2}\left(\frac{Z\alpha}{n}\right)^2. \tag{2.2}$$

with the principal quantum number n. This, however, only describes non-relativistic electrons, which becomes increasingly more inaccurate with higher nuclear charge numbers Z. This can be seen by roughly estimating the velocity of the electron. Adapting a classical picture, the most likely radius to find the electron orbiting the nucleus is at $r_0 = a_0/Z$ with the Bohr radius [8]

$$a_0 = \frac{1}{m_e\alpha}. \tag{2.3}$$

Comparing centripetal forces and the attracting potential, we obtain that

$$\frac{m_e v_0^2}{r_0} = \frac{Ze^2}{4\pi r_0^2}, \tag{2.4}$$

and thus

$$v_0 = Z\alpha. \tag{2.5}$$

This value approaches one, meaning that, in particular for highly charged ions, we need to consider relativistic effects. We, therefore, need to use the stationary Dirac equation.

2.1 Relativistic description of bound electrons

Following Ref. [1], the stationary Dirac equation in a spherically symmetric potential $V(r)$ such as the Coulomb potential is given by

$$(\boldsymbol{\alpha} \cdot \boldsymbol{p} + m_e\beta + V(r))\psi(\boldsymbol{r}) = E\psi(\boldsymbol{r}), \tag{2.6}$$

where c denotes the speed of light, $\psi(\mathbf{r})$, again, the resulting wave function and E the energy eigenvalue. $\boldsymbol{\alpha}$ and β are 4×4 matrices in the form

$$\alpha_i = \begin{pmatrix} 0 & \sigma_i \\ \sigma_i & 0 \end{pmatrix} \qquad \beta = \begin{pmatrix} \mathbb{1} & 0 \\ 0 & -\mathbb{1} \end{pmatrix} \tag{2.7}$$

with σ_i being the Pauli matrices.
To solve the Dirac equation, we can separate the radial and angular dependence of the wave function

$$\psi(\boldsymbol{r}) = \begin{pmatrix} \frac{1}{r}G(r)\Omega_{\kappa m}(\Theta, \phi) \\ \frac{i}{r}F(r)\Omega_{-\kappa m}(\Theta, \phi) \end{pmatrix}. \tag{2.8}$$

The angular dependency is given by the spherical spinors, defined as

$$\Omega_{\kappa m}(\Theta, \phi) = \sum_{m', m_s} C^{j,m}_{l,m';s,m_s} Y_l^{m'}(\Theta, \phi)\chi_{m_s}, \quad \chi_{\frac{1}{2}} = \begin{pmatrix} 1 \\ 0 \end{pmatrix}, \ \chi_{-\frac{1}{2}} = \begin{pmatrix} 0 \\ 1 \end{pmatrix} \tag{2.9}$$

with the Clebsch-Gordan coefficients $C^{j,m}_{l,m';s,m_s}$, the magnetic quantum number m, the orbital quantum number l, the spin quantum number s, the total angular momentum quantum number j and a newly defined quantum number
$\kappa = (j + \frac{1}{2})(-1)^{j+l+\frac{1}{2}}$.
To solve the radial dependence, we can combine Eq. (2.6) and Eq. (2.8) and determine a system of coupled differential equations

$$\frac{dG}{dr} = -\frac{\kappa}{r}G(r) + (E + m_e - V(r))\, F(r) \tag{2.10}$$

$$\frac{dF}{dr} = \frac{\kappa}{r}F(r) - (E - m_e - V(r))\, G(r). \tag{2.11}$$

2.1.1 Solution for point-like nuclei

For point-like nuclei, the potential $V(r)$ is simply the Coulomb potential like in Eq. (2.1)

$$V(r) = -\frac{Z\alpha}{r}. \tag{2.12}$$

Introducing $\lambda = \sqrt{m_e^2 - E^2}$ and $\rho = 2\lambda r$, we can solve Eq. (2.10) and Eq. (2.11) by writing $G(r)$ and $F(r)$ as

$$\begin{pmatrix} G(\rho) \\ F(\rho) \end{pmatrix} = \sqrt{m_e - E^2}\; e^{\frac{1}{2}\rho}\; (\phi_1 \pm \phi_2) \tag{2.13}$$

and assuming $\phi_{1,2}$ to be a power series of the form

$$\phi_1 = \rho^\gamma \sum_{i=1}^{\infty} \alpha_i \rho^i \qquad \phi_2 = \rho^\gamma \sum_{i=1}^{\infty} \beta_i \rho^i, \tag{2.14}$$

where

$$\gamma = \sqrt{\kappa^2 - (Z\alpha)^2} \tag{2.15}$$

and α_i and β_i are recursively defined coefficients. Inserting this into Eq. (2.10) and Eq. (2.11) results in the expression

$$n - |\kappa| + \gamma = \frac{Z\alpha E}{\sqrt{m_e^2 - E^2}} \tag{2.16}$$

and by solving for E we get the Sommerfeld formula describing the eigenenergies

$$E_{\mathrm{Som}} = m_e \left(1 + \frac{(Z\alpha)^2}{\left(n - |\kappa| + \sqrt{\kappa^2 - (Z\alpha)^2} \right)^2} \right)^{\frac{1}{2}}. \tag{2.17}$$

Since the wave function has to be normalised, we can determine the coefficients α_0 and β_0 by solving

$$\int_0^\infty dr \left(F(r)^2 + G(r)^2 \right) = 1. \tag{2.18}$$

This results in the wave functions

$$\begin{aligned} \begin{pmatrix} G(r) \\ F(r) \end{pmatrix} = r \frac{\pm(2\lambda)^{3/2}}{\Gamma(2\gamma+1)} \sqrt{\frac{(m_e \pm E)\Gamma(2\gamma + n - |\kappa| + 1)}{4m_e \frac{Z\alpha m_e}{\lambda} \left(\frac{Z\alpha m_e}{\lambda} - \kappa \right) (n - |\kappa|)}} \rho^{\gamma-1} e^{-\lambda r} \\ \times \left(\left(\frac{Z\alpha m_e}{\lambda} - \kappa \right) {}_1F_1(-n + |\kappa|, 2\gamma + 1; \rho) \right. \\ \left. \mp (n - |\kappa|) {}_1F_1(1 - n + |\kappa|, 2\gamma + 1; \rho) \right) \end{aligned} \tag{2.19}$$

with ${}_1F_1$ being the hypergeometric functions defined as

$$\begin{aligned} {}_1F_1(a,c;x) &= 1 + \frac{a}{c}x + \frac{a(a+1)}{c(c+1)}\frac{x^2}{2!}\cdots \\ &= \sum_{m=0}^{\infty} \frac{a(a+1)\cdots(a+m-1)}{c(c+1)\cdots(c+m-1)}\frac{x^m}{m!}. \end{aligned} \tag{2.20}$$

2.1.2 Solution for extended nuclei

There are different ways to model a finite-sized nucleus. We can achieve a simple and relatively accurate model to solve the Dirac equation for extended nuclei by assuming the charge distribution $\rho(r)$ of a homogeneously charged sphere

$$\rho_{\text{sphere}}(r) = \frac{3Ze}{4\pi r_0^3}\Theta(r_0 - r) \tag{2.21}$$

with the effective radius of the nucleus $r_0 = \sqrt{\frac{5}{3}r_{\text{rms}}^2}$ and the root mean square charge radius given by

$$r_{\text{rms}}^2 = \langle r^2 \rangle = \frac{\int d^3r\ r^2\rho(r)}{\int d^3r\ \rho(r)}. \tag{2.22}$$

This results in a potential of

$$V(r)_{\text{sphere}} = \begin{cases} -\dfrac{Z\alpha}{2r_0}\left(3 - \dfrac{r^2}{r_0^2}\right) & r \leq r_0 \\ -\dfrac{Z\alpha}{2r_0} & r > r_0. \end{cases} \tag{2.23}$$

Following Ref. [9], we can insert this potential into Eq. (2.10) and Eq. (2.11), which leads to two solutions for the radial wave functions. For $r \leq r_0$, we can again assume a power series of the form

$$\begin{pmatrix} G(r) \\ F(r) \end{pmatrix} = r^s \sum_{i=1}^{\infty} (a_i \pm b_i) r^i. \tag{2.24}$$

This results in

$$\begin{pmatrix} G(r) \\ F(r) \end{pmatrix} = N_1 r^{|\kappa|} \sum_{i=1}^{\infty} \left(a_i \pm (-1)^{i+1}\frac{\kappa}{|\kappa|}a_i\right) r^i \tag{2.25}$$

with a free parameter N_1 and recursively defined coefficients a_i

$$a_0 = 1 \tag{2.26}$$

$$a_i = \frac{a_{i-1}\left(E + \frac{3Z\alpha}{2r_0} - m_e(-1)^i \frac{\kappa}{|\kappa|}\right) - \frac{Z\alpha}{2r_0^3} a_{i-3}}{\kappa + (-1)^{i+1}\frac{\kappa}{|\kappa|}(i + |\kappa|)}. \tag{2.27}$$

For $r > r_0$, we can use a similar approach as in Eq. (2.13)

$$\begin{pmatrix} G(\rho) \\ F(\rho) \end{pmatrix} = \sqrt{m_e - E^2}\ \rho^{\frac{1}{2}}\ (\phi_1 \pm \phi_2), \tag{2.28}$$

again using $\rho = 2\lambda r$. This leads to

$$\begin{pmatrix} G(\rho) \\ F(\rho) \end{pmatrix} = \frac{N_2}{\kappa + \frac{m_e Z\alpha}{\lambda}} \rho^{-\frac{1}{2}} \sqrt{m_e \pm E} \times \left(\left(\kappa + \frac{m_e Z\alpha}{\lambda}\right) W_{q,\gamma}(\rho) \pm W_{q+1,\gamma}(\rho)\right) \tag{2.29}$$

with another free parameter N_2 and the Whittaker functions defined as

$$\begin{aligned} W_{q,\gamma}(\rho) = e^{-\frac{\rho}{2}} \rho^{\gamma+\frac{1}{2}} \frac{\Gamma(-2\gamma)}{\Gamma(\frac{1}{2} - \gamma - q)} {}_1F_1(\gamma - q + \frac{1}{2}, 1 + 2\gamma; \rho) \\ + \frac{\Gamma(2\gamma)}{\Gamma(\gamma - q + \frac{1}{2})} \rho^{-2\gamma} {}_1F_1(-\gamma - q + \frac{1}{2}, 1 - 2\gamma; \rho). \end{aligned} \tag{2.30}$$

A more realistic representation of the nucleus can be achieved through the Fermi distribution with the two-parameter form given by

$$\rho_{\text{Fermi}}(r) = Ze \frac{N}{1 + e^{(r-c)/a}}. \tag{2.31}$$

The parameters c and a denote the half-density radius and skin thickness, respectively. The latter is related to $t = 4 \ln 3a$, which is the radial distance over which the charge density falls from 90% to 10% of its value at $r = 0$. For most nuclei, the value $t \approx 2.3$fm is a good approximation [10].
The half-density radius can be described to a good approximation as

$$c^2 = \frac{5}{3} r_{\text{rms}}^2 - \frac{7}{3} a^2 \pi^2. \tag{2.32}$$

The exact value of c can then be determined by finding the root of

$$\frac{\int_0^\infty dr\ r^4 \rho_{\text{Fermi}}(r)}{\int_0^\infty dr\ r^2 \rho_{\text{Fermi}}(r)} - r_{\text{rms}}^2 \tag{2.33}$$

near Eq. (2.32). Furthermore N denotes a normalisation constant approximately given by

$$N = \frac{3}{4\pi c^3}\left(1 + \frac{\pi^2 a^2}{c^2}\right)^{-1} \tag{2.34}$$

and can be determined exactly from the normalisation of the charge distribution. The resulting potential was determined in Ref. [11] and is given by

$$\begin{aligned} V(r)_{\text{Fermi}} = -\frac{Z\alpha}{r}\Bigg[&-\left(\frac{a}{c}\right)^3 S_3\left(-\frac{c}{a}\right) + 6\left(\frac{a}{c}\right)^3 S_3\left(\frac{r-c}{a}\right) \\ &+\frac{r}{c}\left[\frac{3}{2} + \frac{\pi^2}{2}\left(\frac{a}{c}\right)^2 - 3\left(\frac{a}{c}\right)^2 S_2\left(\frac{r-c}{a}\right) - \frac{1}{2}\left(\frac{r}{c}\right)^2\right]\Bigg]. \end{aligned} \tag{2.35}$$

for $x \leq c$ and

$$V(r)_{\text{Fermi}} = -\frac{Z\alpha}{r} - \frac{3Z\alpha}{Kr}\left(\frac{a}{c}\right)^2\left[\frac{r}{c}S_2\left(\frac{c-r}{a}\right) + \frac{2a}{c}S_3\left(\frac{c-r}{a}\right)\right] \tag{2.36}$$

for $x > c$ with

$$K = 1 + \frac{\pi^2 a^2}{c^2} - 6\left(\frac{a}{c}\right)^3 S_3\left(-\frac{c}{a}\right) \tag{2.37}$$

$$S_i(r) = \sum_{n=1}^{\infty} \frac{(-1)^n e^{nr}}{n^i}. \tag{2.38}$$

The wave functions are then determined numerically following the method described in chapter 4.

2.2 Corrections to the energy level from QED

There are QED effects impacting the energy level in Eq. (2.17). At one-loop corrections, the electron can interact with itself by emitting a virtual photon and reabsorbing it. It also interacts with the nucleus by creating and annihilating particle and anti-particle pairs. Figure 2.1 shows the two Feynman diagrams of this interaction.

In this thesis, we will focus on the second phenomenon, which is called vacuum polarisation. To do so, we will look at the interaction between nucleus and electron nonperturbatively and instead assume a classical static external field, similar

(a) Self energy (b) Vacuum polarisation

Figure 2.1: QED corrections to a bound electron, where the double line represents the interaction with the nucleus at all orders and the wave line a virtual photon

to solving the stationary Schrödinger or Dirac equation. We can do so by including the interaction term

$$\mathcal{L}_{ext}(x) = e\bar{\psi}\gamma^{\mu}\mathcal{A}_{\mu}\psi \tag{2.39}$$

directly into the QED Lagrangian [2]

$$\mathcal{L}_{QED+ext} = -\frac{1}{4}F_{\mu\nu}F^{\mu\nu} + \bar{\psi}(i\gamma^{\mu}\partial_{\mu} - m_e - e\gamma^{\mu}\mathcal{A}_{\mu})\psi - eA_{\mu}\bar{\psi}\gamma^{\mu}\psi. \tag{2.40}$$

Here, $\mathcal{A}_{\mu}$ is the classical external vector field representing the effects of the nucleus, whilst A_{μ} is the quantum field operator of the photon. $F^{\mu\nu} = \partial^{\mu}A^{\nu} - \partial^{\nu}A^{\mu}$ is the electromagnetic field operator and γ^{μ} are the Dirac matrices defined as

$$\gamma^0 = \beta \qquad \gamma^i = \beta\alpha^i. \tag{2.41}$$

It can be shown that this is equivalent to describing the interaction between nucleus and electron in the QED picture as an exchange of virtual photons, when assuming that the nucleus is infinitely heavy. A more detailed explanation can be found in Ref. [12].

We can then neglect all terms involving the quantum field operator A^{μ} and solve the resulting Dirac equation, taking the interaction with the nucleus into account in a nonperturbative manner. This approach is called QED in the Furry picture and is further discussed in Ref. [13].

Qualitatively, vacuum polarisation can, therefore, be understood as an external potential U acting on the bound electron. At first order perturbation theory, a shift of the energy level can then be understood by U acting on the wave functions ψ_a, given by

$$\Delta E^{(1)} = \langle\psi_a|U|\psi_a\rangle. \tag{2.42}$$

At higher-order perturbative effects, we will encounter infinite sums over all intermediate wave functions.

At second order, for example, the energy of a bound electron perturbed by an external potential U is given by

$$\Delta E^{(2)} = \sum_{\substack{n \\ n \neq a}} \frac{\langle \psi_a | U | \psi_n \rangle \langle \psi_n | U | \psi_a \rangle}{E_n - E_a}, \tag{2.43}$$

where ψ_n represents all intermediate states.[1] These can be both discrete and continuous, making it either a sum or a normalised integral over the continuous quantum states. In chapter 4, we will briefly outline a possibility to solve these expressions.

2.3 Corrections to the energy level for hyperfine splitting

The Dirac equation only accounts for the binding of the electron to the nucleus. If there are additional external fields, the energy level in Eq. (2.17) is modified. For an external homogeneous magnetic field, this effect is already well known [10]. In this thesis, we will focus on a spherically symmetric field leading to the so called hyperfine splitting.

This phenomenon occurs due to a magnetic moment generated by the spin of the nucleus $\boldsymbol{\mu_I}$ interacting with the magnetic field caused by the rotating electron $\boldsymbol{B_J}$[2]. The interaction Hamiltonian is given by

$$H_{int} = -\boldsymbol{\mu_I} \cdot \boldsymbol{B_J}. \tag{2.44}$$

We use $\boldsymbol{J} = \boldsymbol{L} + \boldsymbol{S}$ to describe the total angular momentum of the electron as the sum of the orbital angular momentum and spin and $\boldsymbol{I}$ to describe the spin of the nucleus. The magnetic moment of the nucleus is determined by its angular momentum $\boldsymbol{I}$

$$\boldsymbol{\mu_I} = g_J \mu_N \frac{\boldsymbol{I}}{\hbar} \tag{2.45}$$

with the nuclear magneton μ_N, defined by the elementary charge e and the proton rest mass m_p

$$\mu_N = \frac{e}{2m_p} \tag{2.46}$$

and the g-factor of the nucleus g_I, which, due to the complex nature of the nucleus, has no accurate theoretical representation.

[1] In chapter 5, we will consider this expression further by looking at vacuum polarisation corrections to the hyperfine splitting.

[2] The reversed view, where the magnetic moment of the electron interacts with the magnetic field caused by the rotating nucleus, would be equally correct, however it's less common.

Using the magnetic potential of a point-like magnetic dipole

$$\boldsymbol{A}(\boldsymbol{r}) = \frac{\boldsymbol{\mu_I} \times \boldsymbol{r}}{4\pi r^3}, \tag{2.47}$$

in order to describe the interaction Hamiltonian as

$$H_{int} = e\ \boldsymbol{\alpha} \cdot \boldsymbol{A} \tag{2.48}$$

we then arrive at the energy shift resulting from this interaction for an electron bound in a state $|\psi\rangle$ as stated in Ref. [14]

$$\Delta E = \langle\psi| e\ \boldsymbol{\alpha} \cdot \boldsymbol{A} |\psi\rangle \tag{2.49}$$

$$\begin{aligned} &= \frac{e}{4\pi} g_I \mu_N \frac{4\kappa}{4\kappa^2 - 1} \left(F(F+1) - I(I+1) - j(j+1)\right) \\ &\quad \times \int_0^\infty \frac{1}{r^2} F_{n\kappa}(r) G_{n\kappa}(r) dr \end{aligned} \tag{2.50}$$

with $F = |I - j|, ..., I + j$.
This integral can be evaluated for point-like nuclei, resulting in the following expression

$$\Delta E = \alpha g_I \frac{m_e}{m_p} \frac{(F(F+1) - I(I+1) - j(j+1))}{2j(j+1)} m_e c^2 \frac{(Z\alpha)^3}{n^3(2l+1)} A(Z\alpha) \tag{2.51}$$

with the "relativistic factor"

$$A(Z\alpha) = n^3(2l+1) \frac{\kappa(2\kappa(\gamma + n - |\kappa|) - N}{N^4 \gamma(4\gamma^2 - 1)} \tag{2.52}$$

further defined in Ref. [15]. γ is given in Eq. (2.15) and

$$N = \sqrt{(n - |\kappa|)^2 + 2(n - |\kappa|)\gamma + \kappa^2}. \tag{2.53}$$

This does not, however, account either for corrections from quantum field theory or for nuclear properties resulting from finite nuclear size when calculating the energy shift. For ground-state electrons in hydrogen-like ions, this can be parameterised as

$$\Delta E^{(1s)} = \Delta E_D^{(1s)} \left(1 - \delta^{(1s)}\right) \left(1 - \varepsilon^{(1s)}\right) + \Delta E_{QED}^{(1s)}, \tag{2.54}$$

where δ accounts for the finite size of the nuclear charge distribution and ε for the finite size of the magnetisation distribution, also called the Bohr-Weisskopf correction. For hydrogen-like ions, these corrections have already been determined in Ref. [10].

$\Delta E_D^{(1s)}$ is the relativistic Dirac value of hyperfine splitting for point-like nuclei and $\Delta E_{QFT}^{(1s)}$ encompasses the possible corrections from quantum field theory. In the

following, we will focus specifically on leptonic and hadronic vacuum polarisation included in the last term.
Inserting the parametrisation into Eq. (2.51) results in the following representation[3]

$$\begin{aligned}\Delta E =& \alpha g_I \frac{m_e}{m_p} \frac{F(F+1) - I(I+1) - j(j+1)}{2j(j+1)} m_e c^2 \\ & \times \frac{(Z\alpha)^3}{n^3(2l+1)} \left(A(Z\alpha)(1-\delta)(1-\varepsilon) + \frac{\alpha}{\pi} \varepsilon_{QFT} \right),\end{aligned} \tag{2.55}$$

where the convention ε_{QFT} is used to denote QFT corrections. It can be determined by comparing Eq. (2.50) and Eq. (2.55).

[3] Additionally, there would be a factor $\mathcal{M}$ accounting for finite nuclear mass if following the parametrisation given in Ref. [10]. It will, however, cancel out at a later time.

3 Vacuum polarisation

As mentioned before, in QED, one of the effects contributing to a shift in energy is vacuum polarisation. It arises from the virtual photon exchanged between two interacting particles decaying into an electron-positron pair that annihilates back into a photon[1].

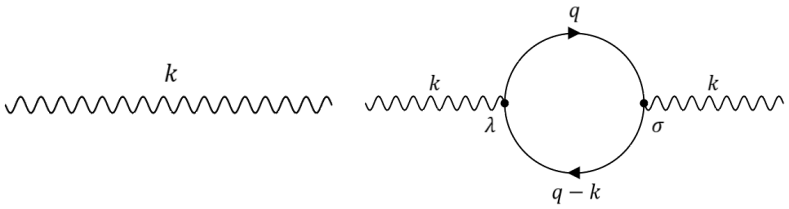

(a) Free photon propagator (b) 1st order correction

Figure 3.1: Feynman diagram of a correction to the photon propagator due to vacuum polarisation

3.1 Modified photon propagator

Following Ref. [5], the free photon propagator in Feynman gauge is described with

$$iD_{\mu\nu}(k) = \frac{-4\pi g_{\mu\nu}}{k^2 + i\epsilon} \tag{3.1}$$

with the four-momentum k and the Minkowski metric tensor $g_{\mu\nu} = \mathrm{diag}(1, -1, -1, -1)$. Including the vacuum polarisation loop as shown in figure 3.1, we can write the modified photon propagator using the Feynman rules

$$iD'_{\mu\nu}(k) = iD_{\mu\nu}(k) + iD_{\mu\lambda}(k)\frac{i\Pi^{\lambda\sigma}(k)}{4\pi}iD_{\sigma\nu}(k) \tag{3.2}$$

[1]This process is not restricted to just electron-positron pairs but can also happen for any particle and antiparticle, as will be discussed later.

with the vacuum polarisation tensor $\Pi^{\lambda\sigma}(k)$

$$\frac{i}{4\pi}\Pi^{\lambda\sigma}(k) = -e^2 \int \frac{d^4q}{(2\pi)^4} \mathrm{Tr}\left(\gamma^\lambda \frac{1}{\not{q} - m_l + i\epsilon} \gamma^\sigma \frac{1}{\not{q} - \not{k} - m_l + i\epsilon}\right), \tag{3.3}$$

where m_l denotes the mass of the particle in the loop and Tr the trace of the matrix resulting from the additional gamma matrices in the Feynman slash notation given by

$$\not{q} = \gamma^\mu q_\mu \tag{3.4}$$

This can also be written in the simplified form

$$\Pi^{\lambda\sigma}(k) = (k^2 g^{\lambda\sigma} - k^\lambda k^\sigma)\Pi(k^2) \tag{3.5}$$

with the divergent vacuum polarisation function $\Pi(k^2)$. After regularisation and charge renormalisation, the divergent part is isolated and we are left with the regular part $\Pi^R(k^2)$.
The modified photon propagator can then be written as

$$D'_{\mu\nu}(k) = -\frac{4\pi g_{\mu\nu}}{k^2} - \frac{4\pi}{k^2}\left(g_{\mu\nu} - \frac{k_\mu k_\nu}{k^2}\right)\Pi^R(k^2). \tag{3.6}$$

3.2 Uehling potential

In order to determine the energy shift, we now want to look at how the Coulomb potential is influenced. The resulting perturbation determines the Uehling potential, which is the shift in potential energy.
The electrostatic scalar potential of the nucleus is given by the convolution of the modified photon propagator $D'_{\mu\nu}(x)$ and current $j_\mu(x)$

$$A'_\mu(x) = \int \frac{d^4x}{(2\pi)^4} D'_{\mu\nu}(k) j^\nu(k) e^{-ikx}. \tag{3.7}$$

Because of the continuity equation $k_\nu j^\nu = 0$, the term containing $k_\mu k_\nu$ in Eq. (3.6) drops out. Furthermore, the nucleus is assumed to be infinitely heavy, allowing us to write the current as

$$j_\mu(x) = -Ze\rho(\boldsymbol{x})\delta_{\mu 0} \tag{3.8}$$

with the nuclear charge density $\rho(\boldsymbol{x})$. Using Fourier transform we can write it in momentum space as

$$j_\mu(k) = -2\pi Ze\ \delta(k_0)\tilde{\rho}(\boldsymbol{k})\delta_{\mu 0}. \tag{3.9}$$

Assuming a point-like nucleus given by $\tilde{\rho}(\boldsymbol{q}) = 1$, we can now write the modified Coulomb potential as

$$\begin{aligned} A_0'(x) &= -Ze \int \frac{d^3x}{(2\pi)^3} \frac{4\pi}{\boldsymbol{k}^2} \tilde{\rho}(\boldsymbol{q}) \left(1 + \Pi^R(-\boldsymbol{k}^2)\right) e^{-ikx} \\ &= -Ze \left(\frac{1}{|\boldsymbol{x}|} + \int \frac{d^3x}{(2\pi)^3} \frac{4\pi}{\boldsymbol{k}^2} \Pi^R(-\boldsymbol{k}^2) e^{-ikx} \right), \end{aligned} \tag{3.10}$$

where the second term is the perturbation arising from vacuum polarisation. For an arbitrary spherical charge distribution, the shift in potential energy, which is simply the perturbated part of the potential multiplied with the elementary charge e, can be written as

$$\delta V(\boldsymbol{x}) = \int \frac{d^3k}{(2\pi)^3} e^{i\boldsymbol{k}\cdot\boldsymbol{x}} \left(-\frac{4\pi e}{\boldsymbol{k}^2} \right) \tilde{\rho}(\boldsymbol{k}) \Pi^R(-\boldsymbol{k}^2). \tag{3.11}$$

Solving the angular integral and redefining $|\boldsymbol{x}| \to r$ and $|\boldsymbol{k}| \to q$, we are left with [5, 16]

$$\delta V(r) = -\frac{2e}{\pi} \int_0^\infty dq \frac{\sin qr}{qr} \tilde{\rho}(q) \Pi^R(-q^2). \tag{3.12}$$

3.3 Leptonic vacuum polarisation

The polarisation function has to be considered for both leptonic and hadronic vacuum polarisation. The first case can be determined analytically and is given by [5]

$$\Pi^R_{\text{lep}}(-q^2) = \frac{2\alpha}{\pi} \int_0^1 d\beta \; \beta(1-\beta) \ln \left[1 + \beta(1-\beta) \frac{q^2}{m_{lep}^2} \right] \tag{3.13}$$

with m_{lep} being the mass of the virtual lepton in the loop.
Following Ref. [2], we can express the Uehling potential in Eq. (3.12) by expanding the integration contour into the imaginary part. Further, if $\beta(1-\beta)q^2/m_{lep}^2 > 1$ the logarithm has a branch cut starting at $q^2 = 4m_{lep}^2$ since $\beta(1-\beta)$ is 1/4 at most. This results in

$$\delta V(r) = -\frac{2\alpha}{\pi r} \int_{2m}^\infty dq \frac{e^{-qr}}{q} \tilde{\rho}(q) \text{Im}[\Pi^R(-q^2 \pm i\varepsilon)] \tag{3.14}$$

with the imaginary part of the vacuum polarisation given by

$$\text{Im}[\Pi^R(-q^2 \pm i\varepsilon)] = \frac{\alpha}{3} \sqrt{1 - \frac{4m_{lep}^2}{q^2}} \left(1 + \frac{2m_{lep}^2}{q^2} \right) \tag{3.15}$$

since $\mathrm{Im}[\ln(-x \pm i\varepsilon)] = \pm\pi$.

3.4 Hadronic vacuum polarisation

For hadronic vacuum polarisation, a perturbative quantum chromodynamic approach fails due to the strong interaction having to be taken into account. Effectively, this means that multiple hadron pairs are already created at first order, making it very difficult to determine the polarisation function. Another possibility to calculate it nevertheless is a semi-empirical approach using experimental data from $e^- e^+ \to$ hadrons collisions.

Following the approach in Ref. [17], we express the real part of the polarisation function with its imaginary part. We can do this using the Kramers-Kronig relations, which can be derived from Cauchy's integral formula and result in

$$\mathrm{Re}[\Pi^R_{\mathrm{had}}(-q^2)] = \frac{q^2}{\pi} P \int_{-\infty}^{+\infty} dq'^2 \frac{\mathrm{Im}[\Pi^R_{\mathrm{had}}(-q'^2)]}{q'^2(q'^2 - q^2 - i\varepsilon)} \tag{3.16}$$

with the principal value integral $P\int_{-\infty}^{+\infty}$.
We can then link this to the measurable total cross section $\sigma_{e^-e^+\to\mathrm{hadrons}}$ using the optical theorem [18]. It can be derived from the unitary property of the scattering matrix and roughly states that the amplitude for an initial state to turn into any other state is proportional to the imaginary part of the process where the final state is equal to the initial state.
In our case, this can be written as

$$\sigma_{e^-e^+\to\mathrm{hadrons}}(q) = \frac{4\pi\alpha}{q^2} \mathrm{Im}[\Pi^R_{\mathrm{had}}(-q^2)]. \tag{3.17}$$

In Ref. [19] data from multiple experiments at different energy regions of centre-of-mass collisions was used to construct an approximate parametrisation of the polarisation function

$$\mathrm{Re}[\Pi^R_{\mathrm{had}}(-q^2)] = A_i + B_i \ln\bigl(1 + C_i|q^2|\bigr) \tag{3.18}$$

with the constants A_i, B_i, C_i defined for different regions of q^2. For our evaluation, we will be using an updated version of these constants, given in table 3.1.
The resulting Uehling potential is given by

$$\delta V_{\mathrm{fns}}(r) = -\frac{2e}{\pi} \sum_{i=1}^{7} \left[\int_{k_i - 1}^{k_i} dq \frac{\sin qr}{qr} \tilde{\rho}(q) [A_i + B_i \ln\bigl(1 + C_i|q^2|\bigr)] \right]. \tag{3.19}$$

As stated in Ref. [6], using only the parameters of the first momentum region up to infinity is accurate enough up to $Z = 96$ at least. For a point-like nucleus, the

Table 3.1: Values for the parametrisation of the hadronic vacuum polarisation function with the mass of the Z boson m_Z [20]

Region	Range (GeV)	A_i	B_i	C_i (GeV^{-2})
$k_0 - k_1$	0.0-0.7	0.0	0.0023092	3.9925370
$k_1 - k_2$	0.7-2.0	0.0	0.0023333	4.2191779
$k_2 - k_3$	2.0-4.0	0.0	0.0024402	3.2496684
$k_3 - k_4$	4.0-10.0	0.0	0.0027340	2.0995092
$k_4 - k_5$	10.0-m_Z	0.0010485	0.0029431	1.0
$k_5 - k_6$	m_Z-10^4	0.0012234	0.0029237	1.0
$k_6 - k_7$	10^4-10^5	0.0016894	0.0028984	1.0

Uehling potential then simplifies to

$$\begin{aligned}\delta V_{\text{point}}^{\text{approx}}(r) &= -\frac{2Z\alpha}{\pi}\int_0^\infty dq \frac{\sin qr}{qr}[B_1 \ln\big(1 + C_1|q^2|\big)] \\ &= \frac{2Z\alpha}{r} B_1 E_1\left(\frac{r}{\sqrt{C_1}}\right)\end{aligned} \tag{3.20}$$

with the exponential integral

$$E_n(x) = \int_1^\infty dt \frac{e^{-xt}}{t^n}. \tag{3.21}$$

For an extended nucleus the Uehling potential can be calculated by convoluting the point-like Uehling potential with the charge distribution $\rho(\boldsymbol{r})$ [6]

$$\delta V_{\text{fns}}^{\text{approx}}(\boldsymbol{r}) = \frac{1}{Z\alpha}\int d^3x\ \rho(\boldsymbol{x})\delta V_{\text{point}}^{\text{approx}}(\boldsymbol{r} - \boldsymbol{x}). \tag{3.22}$$

Inserting the approximated potential into Eq. (3.20) and a spherically symmetric charge distribution results in

$$\delta V_{\text{fns}}^{\text{approx}}(r) = -\frac{4\pi e B_1\sqrt{C_1}}{r}\int_0^\infty dx\ x\rho(x)D_2^-(r,x) \tag{3.23}$$

with

$$D_n^\pm(r,x) = E_n\left(\frac{|r-x|}{\sqrt{C_1}}\right) \pm E_n\left(\frac{|r+x|}{\sqrt{C_1}}\right). \tag{3.24}$$

Depending on the nuclear model, we can now insert Eq. (2.21) or (2.31) into $\rho(x)$.

4 Numerical methods

In order to perform numerical calculations, we need a way to parameterise the wave functions through smooth and continuous curves. However, that becomes increasingly more difficult the more intricately a curve is shaped. In the following section, we will briefly discuss a method widely used to parameterise all kinds of curves.

4.1 From Bézier curves to B-splines

The basis for this explanation are Bézier curves. They are generated by connecting two points P_0 and P_1 with a straight line. On this line, another point A is defined, whose position is parameterised with a value $t = [0, 1]$. For $t = 0$, A is at P_0, for $t = 1$ at P_1 and for $t = 0.5$ in the middle of both points. Mathematically, this can be written as

$$A = (1 - t)P_0 + tP_1. \tag{4.1}$$

If we add another point P_2 and connect it to P_1, we can again parameterise a point B with the same value for t. A and B can now be connected, as well ,with another point P, following the same parameterisation. The path this point takes when letting t go from 0 to 1 is a smooth curve no matter where the control points P_0, P_1, P_2 are located. This path is called a quadratic Bézier curve and can be written in terms of each point

$$\begin{aligned} A &= (1 - t)P_0 + tP_1 \\ B &= (1 - t)P_1 + tP_2 \end{aligned} \tag{4.2}$$

$$P(t) = (1 - t)A + tB = P_0(t^2 - 2t + 1) + P_1(-2t^2 + 2t) + P_2t^2. \tag{4.3}$$

In this representation, the points P_0 to P_2 can be interpreted as vectors from an arbitrary origin point which are then added together, whilst the polynomials determine how much weight these points carry for each sector of the curve. Each of these weights added together always add up to 1 at any given t-value. At $t = 0$, the first weight is one and as t increases, the values shift across the points until the last weight is one. In practice, there is usually another control point P_3 added. By repeating the process of connecting two points next to each other until there is only one left, we then get the cubic Bézier curve. Using matrix notation and following

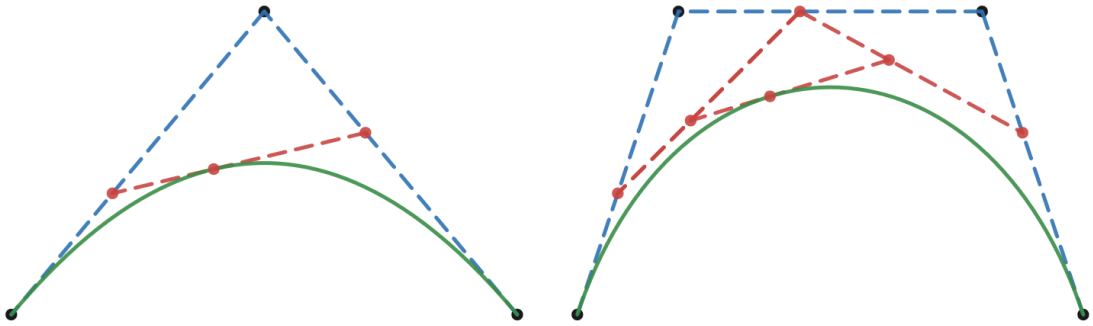

(a) Quadratic Bézier curve (b) Cubic Bézier curve

Figure 4.1: Bézier curves (green) with their control points (black). The red dots and the red lines connecting them demonstrate how the curve is parameterised at $t = 0.4$.

Eq. (4.3) we can write the polynomial as

$$P(t) = \begin{pmatrix} 1 & t & t^2 & t^3 \end{pmatrix} \begin{pmatrix} 1 & 0 & 0 & 0 \\ -3 & 3 & 0 & 0 \\ 3 & -6 & 3 & 0 \\ -1 & 3 & -3 & 1 \end{pmatrix} \begin{pmatrix} P_0 \\ P_1 \\ P_2 \\ P_3 \end{pmatrix}. \tag{4.4}$$

For more complicated curves, we can simply add more control points, however that method quickly becomes unstable, or at least very expensive to calculate. Furthermore, the resulting curve does not pass through most points, making it difficult to parameterise. Additionally, there is no local control since changing just one point has an impact on the entire curve.
To solve that problem, we can simply add multiple cubic Bézier curves to each other, forming the Bézier splines. The resulting curve can be controlled locally since changing one control point only affects the corresponding Bézier curve. It is easier to parameterise since it passes through every third control point and the calculations do not get more expensive by adding more points because only one cubic Bézier curve is sampled. The weights can also be attached to each other, resulting in the basis function of the spline. This basis function, and thus the curve itself, is C^0 continuous, however it already fails at C^1 continuity. For each order of continuity we have to introduce a constraint to the control points, which again leads to a loss of local control.

We, therefore, need to modify the matrix in Eq. (4.4) such that the four weights attached to each other result in a C^2 continuous basis function. Taking into account that all weights added together still have to equal one, this results in 16 boundary

conditions. This allows us to solve for the 16 unknowns in the matrix, resulting in

$$P(t) = \begin{pmatrix} 1 & t & t^2 & t^3 \end{pmatrix} \frac{1}{6} \begin{pmatrix} 1 & 4 & 1 & 0 \\ -3 & 0 & 3 & 0 \\ 3 & -6 & 3 & 0 \\ -1 & 3 & -3 & 1 \end{pmatrix} \begin{pmatrix} P_0 \\ P_1 \\ P_2 \\ P_3 \end{pmatrix}. \tag{4.5}$$

The resulting spline is called a B-spline (Basis-spline). An example can be seen in figure 4.2, where one control point was changed in order to illustrate its local effect on the adjacent curve segments. We can see that, in general, the spline does not go through the control points any more, but it is still C^2 continuous and there is local control.

When using the spline in calculations it is usually defined through its order K, which, in our case so far, has been 3 and the number of control points N. We have, therefore, generated a way to describe the wave functions using only certain control points.

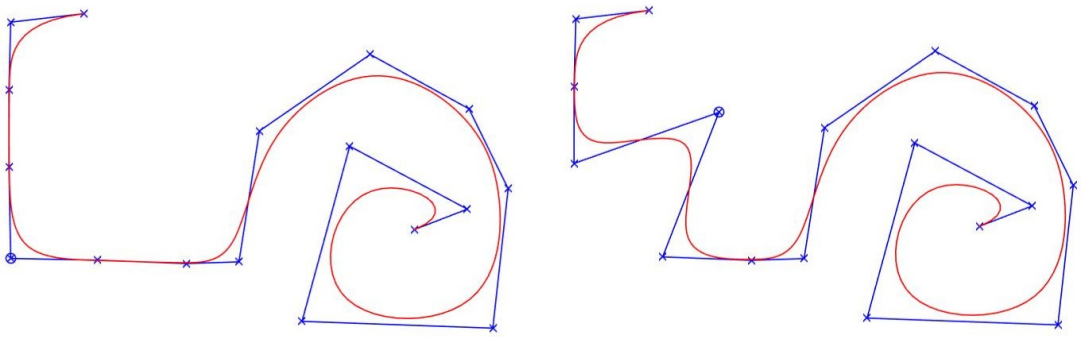

Figure 4.2: B-spline of order $K = 3$ with $N = 17$ control points with one control point changed for comparison (plot has been created in Matlab [21])

4.2 The Dirac equation in a finite basis set

The radial Dirac equation, given by Eq. (2.6), can be written as

$$H\phi = E\phi, \tag{4.6}$$

where ϕ is the vector of the radial functions $G(r)$ and $F(r)$ and

$$H = \begin{pmatrix} V + m_e & c\left(\frac{\kappa}{r} - \frac{d}{dr}\right) \\ c\left(\frac{\kappa}{r} + \frac{d}{dr}\right) & V - m_e \end{pmatrix}. \tag{4.7}$$

Given any vector ϕ, the Dirac equation can then be derived by variation of the action

$$S(\phi) = \langle\phi|H|\phi\rangle - E\langle\phi|\phi\rangle \tag{4.8}$$

if $G(r)$ and $F(r)$ hold proper boundary conditions.
Following Ref. [22], let us consider such a system confined to a spherical cavity of radius R_{cav}. This imposes boundary conditions on the wave function at $r = 0$ and $r = R_{cav}$, making it possible for us to describe it solely discretely.
We can, therefore, approximate ϕ by a finite linear combination of basis vectors u_i satisfying the boundary conditions and coefficients c_i given by

$$\phi(r) = \sum_{i=1}^{2N} c_i u_i(r). \tag{4.9}$$

We can substitute this into Eq. (4.8) and, since solutions to the Dirac equation are stationary points of the action, the variation of the action reduces to

$$\frac{dS}{dc_i} = 0, \qquad i = 1, 2, ..., 2N. \tag{4.10}$$

This can be written as

$$\boldsymbol{A} \cdot \boldsymbol{c} = E\ \boldsymbol{B} \cdot \boldsymbol{c} \tag{4.11}$$

with the components of the $2N \times 2N$ matrices $\boldsymbol{A}$ and $\boldsymbol{B}$

$$A_{ij} = \frac{\langle u_i|H|u_j\rangle + \langle u_j|H|u_i\rangle}{2} \tag{4.12}$$

$$B_{ij} = \langle u_i|u_j\rangle. \tag{4.13}$$

Solving Eq. (4.11) results in eigenvalues E_i and coefficients $\boldsymbol{c}(i)$.[1]
This means that the radial wave functions can now be approximated numerically by the vector of coefficients $\boldsymbol{c}(i)$, and corrections to these wave functions can also be described as corrections to the coefficients.
Eq. (2.43) can now be solved by writing it as

$$\Delta E = \langle\psi_a|U|\delta\psi_a\rangle \tag{4.14}$$

with

$$|\delta\psi_a\rangle = \sum_{\substack{n \\ E_n \neq E_a}} \frac{\langle\psi_n|U|\psi_a\rangle}{E_n - E_a}|\psi_n\rangle. \tag{4.15}$$

[1] For $i = 1, ..., N$, the negative continuum is approximated and for $i = N + 1, ..., 2N$, the positive continuum and the bound states are approximated.

Assuming a spherically symmetric potential, only the radial part of this corrected wave function is influenced since the relativistic angular momentum and magnetic quantum numbers are preserved. As discussed above, this correction can then be described entirely by correcting the coefficients. We are now left only with determining the basis functions $u_i(r)$, which we will achieve through B-splines.

4.3 Calculations using B-splines

In order to calculate the basis vectors $u_i(r)$ introduced in Eq. (4.9), we first have to mathematically describe B-splines using the definitions described in Ref. [22, 23].

First, the values for t now go through $[t_0, t_{N+K}]$ instead of $[0, 1]$ and, to follow convention, we will rename $t \to r$.
The equation for the B-spline functions at control point i are denoted recursively with the function of order one defined as

$$B_{i1}(r) = \begin{cases} 1, & t_i \leq r < t_{i+1} \\ 0, & \text{otherwise} \end{cases} \tag{4.16}$$

and the following functions of order K defined as

$$B_{iK}(r) = \frac{r - t_i}{t_{i+K-1} - t_i} B_{i,K-1}(r) + \frac{t_{i+K} - r}{t_{i+K} - t_{i+1}} B_{i+1,K-1}(r). \tag{4.17}$$

This means that B_{iK} vanishes outside of the intervals $t_i \leq r < t_{i+K}$, which is why we have local control over the curve. For our calculations, the knots t_i are chosen such that $t_1 = ... = t_K = 0$ and $t_{N+1} = ... = t_{N+K} = R_{\text{cav}}$.

Following Ref. [22], the so-called dual kinetic balance (DKB) approach is used, which allows a description of extended nuclei without the occurrence of spurious states. It describes a basis set given by

$$u_i(r) = \begin{pmatrix} B_i(r) \\ \frac{1}{2m_e}\left(\frac{d}{dr} + \frac{\kappa}{r}\right) B_i(r) \end{pmatrix} \qquad i = 1, ..., N \tag{4.18}$$

$$u_i(r) = \begin{pmatrix} \frac{1}{2m_e}\left(\frac{d}{dr} - \frac{\kappa}{r}\right) B_{i-N}(r) \\ B_{i-N}(r) \end{pmatrix} \qquad i = N+1, ..., 2N. \tag{4.19}$$

The resulting radial wave functions, expressed by b-spline basis functions are given

by

$$G_{n\kappa(r)} = \sum_{i=2}^{N-1} \left[c_i(n\kappa) B_i(r) + \frac{c_{N+i}(n\kappa)}{2m_e} \left(B_i'(r) - \frac{\kappa}{r} B_i(r) \right) \right] \tag{4.20}$$

$$F_{n\kappa}(r) = \sum_{i=2}^{N-1} \left[\frac{c_i(n\kappa)}{2m_e} \left(B_i'(r) - \frac{\kappa}{r} B_i(r) \right) + c_{N+i}(n\kappa) B_i(r) \right]. \tag{4.21}$$

Our calculations where then performed by modifying the code introduced in [24].

5 Second-order corrections

So far, we have regarded hyperfine splitting and vacuum polarisation as two distinct corrections to the energy level.

At first order, the energy shift resulting from both effects can be denoted as

$$\Delta E^{(1)}_{n\kappa} = \langle \psi_{n\kappa} | V_{\mathrm{Ueh}} | \psi_{n\kappa} \rangle + \langle \psi_{n\kappa} | V_{\mathrm{mag}} | \psi_{n\kappa} \rangle. \tag{5.1}$$

However, at second order, one has to regard their interaction as well.

There are two different ways the effects can interact which can be seen in figure 5.1, where vacuum polarisation either impacts the wave function or changes the magnetic potential directly.

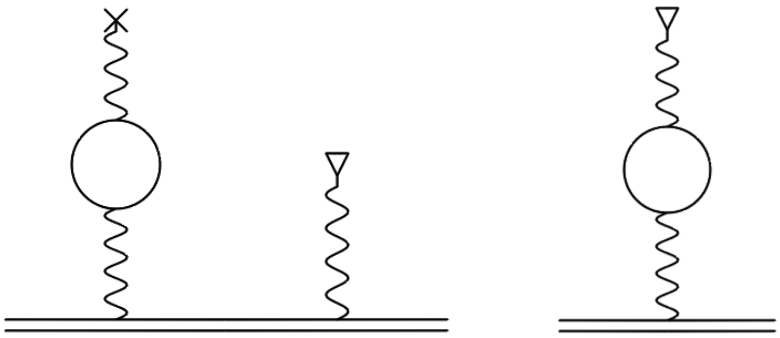

(a) Correction to the wave function (b) Correction to the potential

Figure 5.1: Second order corrections to the energy level of a bound electron (represented by the double line) regarding hyperfine splitting and vacuum polarisation.[1]

5.1 Correction to the wave function

In the first case, the wave function directly interacts with both the Uehling potential and the magnetic potential. At second order, we can, therefore, write the energy

[1] In this case the circle represents both leptonic and hadronic vacuum polarisation

shift as

$$\Delta E_{1s}^{(2)} = 2 \sum_{\substack{n' \\ n \neq n'}} \frac{\langle \psi_{n\kappa} | V_{\mathrm{Ueh}} | \psi_{n'\kappa} \rangle \langle \psi_{n'\kappa} | V_{\mathrm{mag}} | \psi_{n\kappa} \rangle}{E_{n\kappa} - E_{n'\kappa}} \tag{5.2}$$

with a factor 2, due to an identical contribution with the potentials interchanged. Due to the spherically symmetrical nature of the magnetic potential, the integral over the angular components can be evaluated similarly to Eq. (2.55), therefore allowing us to write it as

$$\begin{aligned} \Delta E_{1s}^{(2)} = 2 \sum_{\substack{n' \\ n \neq n'}} & \frac{\langle \psi_{n\kappa} | V_{\mathrm{Ueh}} | \psi_{n'\kappa} \rangle}{E_{n\kappa} - E_{n'\kappa}} \left(- \frac{2\alpha g_I (F(F+1) - I(I+1) - j(j+1))}{3 m_p} \right) \\ & \times \int_0^\infty dr \frac{1}{r^2} (F_{n'\kappa}(r) G_{n\kappa}(r) + G_{n'\kappa} F_{n\kappa}). \end{aligned} \tag{5.3}$$

Comparing both equations, we are left with

$$m_e^2 (Z\alpha)^3 \frac{\alpha}{\pi} \varepsilon_{\mathrm{VP}} = - \sum_{\substack{n \\ n' \neq n}} \frac{\langle \psi_{n\kappa} | V_{\mathrm{Ueh}} | \psi_{n'\kappa} \rangle}{E_{n\kappa} - E_{n'\kappa}} \int_0^\infty dr \frac{1}{r^2} (F_{n'\kappa}(r) G_{n\kappa}(r) + G_{n'\kappa} F_{n\kappa}). \tag{5.4}$$

As stated in Eq. (4.14), we can write the right-hand side of this expression as

$$- \langle \psi_{n\kappa} | V_{\mathrm{Ueh}} | \delta\psi_{\mathrm{mag}} \rangle, \tag{5.5}$$

where we have pulled the sum into the expression $\delta\psi_{mag}$. It describes the magnetically disturbed wave function and for point-like nuclei, following the derivation in Ref. [25], it can be written as

$$\delta\psi_{\mathrm{mag}} = \begin{pmatrix} i X_{\mathrm{mag}}(r) \Omega_{\kappa m} \\ - Y_{\mathrm{mag}}(r) \Omega_{\kappa m} \end{pmatrix}. \tag{5.6}$$

A more detailed explanation as well as an analytic expression for $X(r)$ and $Y(r)$ can be found in Appendix B. For extended nuclei, the method discussed in chapter 4 is used.
By solving the angular integration, we can describe the correction to the energy shift as

$$\varepsilon^{\mathrm{wf,pl}} = - \frac{\pi}{\alpha} \frac{\int dr V_{\mathrm{Ueh}}(r) \left(G_{n\kappa}(r) X_{\mathrm{mag}}(r) + F_{n\kappa}(r) Y_{\mathrm{mag}}(r) \right)}{m_e^2 (Z\alpha)^3}. \tag{5.7}$$

For extended nuclei, we calculate the correction numerically using B-splines. The approach is similar, however the perturbated wave function is computed with the

Uehling potential as the perturbation potential U in Eq. (4.15)

$$\Delta E^{(2)}_{n\kappa} := 2\langle\psi_{n\kappa}|\delta V_{\mathrm{mag}}|\delta\psi_{\mathrm{Ueh}}\rangle. \tag{5.8}$$

The correction to the energy level can then be determined analogously to Eq. (5.7) with

$$\varepsilon^{\mathrm{wf,fns}} = -\frac{\pi}{\alpha}\frac{\int dr V_{\mathrm{mag}}(r)\left(G_{n\kappa}(r)X_{\mathrm{Ueh}}(r) + F_{n\kappa}(r)Y_{\mathrm{Ueh}}(r)\right)}{m_e^2(Z\alpha)^3}. \tag{5.9}$$

5.2 Correction to the magnetic potential

Now, we regard the correction to the magnetic potential. In momentum space we can write the modified potential simply as a multiplication of the polarisation functions determined in Eq. (3.15) and (3.18) and the magnetic potential of the hyperfine structure

$$\boldsymbol{A}_{\mathrm{ML}}(\boldsymbol{q}) = \Pi^R(-q^2)\boldsymbol{A}(\boldsymbol{q}) \tag{5.10}$$

with the index ML denoting the magnetic loop corrected potential and [10]

$$\boldsymbol{A}(\boldsymbol{q}) = -\frac{i}{(2\pi)^3}\frac{\boldsymbol{\mu_I}\times\boldsymbol{q}}{q^2}. \tag{5.11}$$

The resulting potential is then determined by introducing the Fourier transform

$$\boldsymbol{A}_{\mathrm{ML}}(\boldsymbol{r}) = \int\frac{d^3q}{(2\pi)^3}e^{i\boldsymbol{qr}}\Pi^R(-q^2)(-i)\frac{\boldsymbol{\mu_I}\times\boldsymbol{q}}{q^2}. \tag{5.12}$$

Following Ref. [26], we can now use the fact that

$$i\nabla_{\boldsymbol{s}}e^{-i\boldsymbol{qs}}|_{\boldsymbol{s}=0} = \boldsymbol{q} \tag{5.13}$$

and write the potential as

$$\boldsymbol{A}_{\mathrm{ML}}(\boldsymbol{r}) = -i\boldsymbol{\mu_I}\times\left(i\nabla_{\boldsymbol{s}}\int\frac{d^3q}{(2\pi)^3}e^{i\boldsymbol{q}(\boldsymbol{r}-\boldsymbol{s})}\frac{\Pi^R(-q^2)}{q^2}\right)\Bigg|_{\boldsymbol{s}=0}. \tag{5.14}$$

For leptonic vacuum polarisation, this was determined in Ref. [26] to be

$$\boldsymbol{A}_{\mathrm{ML,lep}}(\boldsymbol{r}) = \boldsymbol{A}(\boldsymbol{r})\frac{2\alpha}{3\pi}\int_1^\infty dz\sqrt{1-\frac{1}{z^2}}\left(1+\frac{1}{2z^2}\right)\frac{1}{z}e^{-2mrz}(2mrz+1). \tag{5.15}$$

In case of hadronic vacuum polarisation, we can carry out the angular integration in Eq. (5.14) resulting in

$$\int \frac{d^3q}{(2\pi)^3} e^{i\boldsymbol{q}(\boldsymbol{r}-\boldsymbol{s})} \frac{\Pi^R(q^2)}{q^2} = \frac{1}{2\pi^2 R} \int_0^\infty dq \frac{\sin qR}{q^2} \Pi^R(-q^2) \tag{5.16}$$

with $R = |\boldsymbol{R}| = |\boldsymbol{r} - \boldsymbol{s}|$ and $q = |\boldsymbol{q}|$. Following Eq. (3.20), we can write Eq. (5.14) as

$$\boldsymbol{A}_{\mathrm{ML,had}}(\boldsymbol{r}) = -i\boldsymbol{\mu_I} \times \left(i\nabla_{\boldsymbol{s}} \frac{B}{2\pi R} \int_1^\infty dt \frac{e^{\frac{R}{\sqrt{C}}t}}{t} \right) \Bigg|_{\boldsymbol{s}=0}. \tag{5.17}$$

This, we can now solve and by renaming $R \to r$ we get

$$\boldsymbol{A}_{\mathrm{ML,had}}(\boldsymbol{r}) = \boldsymbol{A}(\boldsymbol{r}) 2B \left(e^{-\frac{r}{\sqrt{C}}} + E_1\left(\frac{r}{\sqrt{C}}\right) \right). \tag{5.18}$$

As we can see from Eq. (5.15) and (5.18), we can simply introduce a factor $F_{ML}(r)$ to account for the magnetic loop

$$\boldsymbol{A}_{\mathrm{ML}}(\boldsymbol{r}) = \frac{\boldsymbol{\mu_I} \times \boldsymbol{r}}{4\pi r^3} F_{\mathrm{ML}}(r). \tag{5.19}$$

Since this factor is spherically symmetric the angular integration stays the same and Eq. (2.50) can be written as

$$\begin{aligned} \Delta E_{\mathrm{ML}} =& \frac{e}{4\pi} g_I \mu_N \frac{4\kappa}{4\kappa^2 - 1} \left(F(F+1) - I(I+1) - j(j+1)\right) \\ & \times \int_0^\infty dr \frac{1}{r^2} G_{n\kappa}(r) F_{n\kappa}(r) F_{\mathrm{ML}}(r), \end{aligned} \tag{5.20}$$

resulting in the energy correction of

$$\varepsilon^{\mathrm{pot,fns}} = \frac{\pi}{\alpha} \frac{\int dr \frac{1}{r^2} G_{n\kappa}(r) F_{n\kappa}(r) F_{\mathrm{ML}}(r)}{m_e^2 (Z\alpha)^3}. \tag{5.21}$$

This correction was calculated for the bound electron's wave functions of point-like, sphere and Fermi distributed nuclei.

5.3 Results

Using the atomic radii listed in appendix A, we can now calculate the values of ε for corrections to the wave function (wf) and the magnetic potential (mag) in case of point-like nuclei (pl) and extended nuclei (fns) for the discussed nuclear models (sphere, fermi). The uncertainty of the given values arises from the uncertainty of the rms radius of the isotopes. The results can be seen in table 5.3.

Table 5.1: Electronic vacuum polarisation corrections for 1s states.

Z	$\varepsilon_{el}^{wf,pl}$	$\varepsilon_{el}^{pot,pl}$	$\varepsilon_{el,\mathrm{sphere}}^{wf,fns}$	$\varepsilon_{el,\mathrm{fermi}}^{wf,fns}$	$\varepsilon_{el,\mathrm{sphere}}^{pot,fns}$	$\varepsilon_{el,\mathrm{fermi}}^{pot,fns}$	Refs.
1	0.0087703	0.0085579	0.0086376(11)		0.0084255(12)		
	0.0087691	0.0085578					[10]
	0.0087703	0.0085578					[27]
2	0.01781815	0.0170486	0.01736232(63)		0.01659564(62)		
	0.017817	0.017049					[10]
4	0.0366463	0.0338856	0.0353555(50)	0.0354155(54)	0.0326152(49)	0.0326751(53)	
	0.036645	0.033886					[10]
5	0.046415	0.042257	0.044833(26)	0.044913(29)	0.040708(26)	0.040787(28)	
	0.046414	0.042257					[10]
	0.0464153	0.0422566					[27]
10	0.0989572	0.0840724	0.0949078(23)	0.0950343(24)	0.0802593(21)	0.0803801(22)	
	0.098955	0.084072	0.094922		0.080275		[10]
	0.0989572	0.0840724					[27]
25	0.3068919	0.2192739	0.2887396(81)	0.2890727(84)	0.2051510(64)	0.2054255(66)	
	0.3068919	0.2192738					[27]
44	0.794009	0.458597	0.706157(25)	0.707029(26)	0.409936(15)	0.410497(15)	
			0.7065		0.4102		[10]
63	2.04367	0.91404	1.59915(42)	1.60183(30)	0.74805(18)	0.74932(12)	
				1.59		0.73	[10]
70	3.04459	1.21160	2.17126(49)	2.17517(46)	0.93193(17)	0.93360(18)	
83	7.43667	2.24726	4.03804(52)	4.04772(52)	1.45440(15)	1.45768(15)	
			4.038	4.05	1.455	1.46	[10]
92	16.9325	3.92182	6.3778(13)	6.3956(14)	2.01655(33)	2.02169(33)	
			6.377		2.016		[10]

Table 5.2: Muonic vacuum polarisation corrections for 1s states.

Z	$\varepsilon_{mu}^{wf,pl}$	$\varepsilon_{mu}^{pot,pl}$	$\varepsilon_{mu,\mathrm{sphere}}^{wf,fns}$	$\varepsilon_{mu,\mathrm{fermi}}^{wf,fns}$	$\varepsilon_{mu,\mathrm{sphere}}^{pot,fns}$	$\varepsilon_{mu,\mathrm{fermi}}^{pot,fns}$
1	0.00004162	0.000041604	0.00001655(10)		0.000016543(98)	
2	0.000083427	0.000083359	0.000021298(28)		0.000021269(28)	
4	0.00016827	0.00016786	0.00003060(13)	0.00003413(17)	0.00003049(13)	0.00003402(18)
5	0.00021161	0.00021086	0.00003968(74)	0.00004460(97)	0.00003951(72)	0.00004442(98)
10	0.000444046	0.000438598	0.000067984(43)	0.000073562(54)	0.000067246(43)	0.000072809(54)
25	0.00151814	0.001413614	0.00017115(10)	0.00018059(12)	0.000164787(94)	0.00017410(11)
44	0.00573678	0.00458894	0.00038522(18)	0.00039987(20)	0.00035179(17)	0.00036593(18)
63	0.0283835	0.0174905	0.0009377(20)	0.0009676(14)	0.0007954(17)	0.0008233(13)
70	0.0579742	0.0312626	0.0012740(18)	0.0013098(20)	0.0010441(15)	0.0010769(17)
83	0.2880179	0.1119933	0.0026262(17)	0.0026961(18)	0.0020019(13)	0.0020633(14)
92	1.1990217	0.3390947	0.0043050(36)	0.0044087(38)	0.0030906(26)	0.0031785(28)

Table 5.3: Hadronic vacuum polarisation corrections for 1s states.

Z	$\varepsilon_{had}^{wf,pl}$	$\varepsilon_{had}^{pot,pl}$	$\varepsilon_{had,\mathrm{sphere}}^{wf,fns}$	$\varepsilon_{had,\mathrm{fermi}}^{wf,fns}$	$\varepsilon_{had,\mathrm{sphere}}^{pot,fns}$	$\varepsilon_{had,\mathrm{fermi}}^{pot,fns}$
1	0.00005931	0.00005930	0.00001385(11)		0.00001384(11)	
2	0.000118901	0.000118827	0.000015720(24)		0.000015700(24)	
4	0.000239897	0.0002394018	0.000021458(99)	0.00002462(15)	0.000021386(99)	0.00002455(15)
5	0.00030178	0.00030085	0.00002793(56)	0.00003242(84)	0.00002781(57)	0.00003230(84)
10	0.000634961	0.0006276924	0.000046964(32)	0.000051587(43)	0.0000464885(32)	0.000051104(42)
25	0.002215687	0.002066843	0.000116714(70)	0.000123978(84)	0.000112649(69)	0.000119854(82)
44	0.00883423	0.00708513	0.00026054(13)	0.00027125(14)	0.00023910(12)	0.00024956(13)
63	0.0477348	0.0294996	0.0006323(13)	0.0006538(10)	0.0005407(12)	0.00056110(91)
70	0.1017223	0.0550071	0.0008576(13)	0.0008830(14)	0.0007090(11)	0.0007327(12)
83	0.5559891	0.21670903	0.0017666(12)	0.0018158(13)	0.00136180(92)	0.0014062(10)
92	2.5102986	0.7112905	0.0028925(25)	0.0029648(26)	0.0021021(18)	0.0021652(19)

For point-like nuclei and small charge numbers, we can use approximate formulas to compare to our results similar to [28]. We do so by first approximating the free and magnetically perturbated radial wave functions in the lowest order of $Z\alpha$, as well as their product

$$\begin{aligned} G(r) &\approx r2(m_e Z\alpha)^{\frac{3}{2}} e^{-m_e Z\alpha r}, \\ F(r) &\approx 0, \\ X_{mag}(r) &\approx G(r), \\ G(r)F(r) &\approx -2m_e^3 (Z\alpha)^4 e^{-2\lambda r}. \end{aligned} \tag{5.22}$$

Inserting these expressions into Eq. (5.7) and Eq. (5.21) results in the same expression. For leptonic VP, it is given by

$$\varepsilon_{\text{approx}}^{\text{lep,pl}} = \frac{3}{8}\pi Z\alpha \frac{m_e}{m_{lep}}, \tag{5.23}$$

to which our results for electronic VP coincide within the first digit up until $Z = 5$ for the corrected wave function and $Z = 25$ for the corrected magnetic potential. For muonic VP, it coincides up until $Z = 25$ in both cases. For hadronic VP, it is given by

$$\varepsilon_{\text{approx}}^{\text{had,pl}} = 8\pi m_e Z B\sqrt{C}, \tag{5.24}$$

coinciding within the first digit up until $Z = 4$.

In table 5.5, the differences between the different nuclear models are listed, illustrating that the results are extremely sensitive to the nuclear model used.
It was expected that the solutions for point-like nuclei would differ more with increasing Z. However, for muonic and hadronic vacuum polarisation there is already a discrepancy in the first digit between point-like and fns solutions. This suggests that the vacuum polarisation itself might already take place within the nucleus, or at least be significantly closer to it, than when considering corrections due to a homogeneous external field. This is further supported when considering table 5.8, where the values for $2s$ electrons are listed. Here, the effect, whilst still notable, is not as prominent anymore since the $2s$ electrons are further away from the nucleus. These results, therefore, show that when considering hyperfine effects, it is necessary to have a better understanding of the nuclear model.

It is also interesting to consider $2s$ states, given in table 5.8, since they can be a first approximation for lithium-like systems, where there are two electrons occupying the $1s$ state and one electron in the $2s$ state. The $1s$ electrons shield the effect of the nucleus to some extent, allowing us to treat the external electron in a lithium-like system with nuclear charge number Z like a $2s$ electron in a hydrogen-like system with nuclear charge $Z-2$. When calculating these $2s$ states, we have to account for a factor of 8 due to Eq. (2.55) being proportional to $1/n^3$.

However, as seen with the effect different nuclear models had on the results, this

Table 5.4: Dependence on the nuclear model for corrected wave function.

Z	$\Delta\varepsilon_{el}^{pl-\text{sphere}}$	$\Delta\varepsilon_{mu}^{pl-\text{sphere}}$	$\Delta\varepsilon_{had}^{pl-\text{sphere}}$	$\Delta\varepsilon_{el}^{\text{fermi-sphere}}$	$\Delta\varepsilon_{mu}^{\text{fermi-sphere}}$	$\Delta\varepsilon_{had}^{\text{fermi-sphere}}$
1	0.0001327(11)	0.00002507(10)	0.00004546(11)			
2	0.00045583(63)	0.000062129(28)	0.000103181(24)			
4	0.0012908(50)	0.00013767(13)	0.000218439(99)	0.000060(10)	0.0000035(34)	0.00000320(25)
5	0.001582(26)	0.00017193(74)	0.00027385(56)	0.000080(55)	0.0000049(17)	0.0000046(14)
10	0.0040494(23)	0.000376062(43)	0.000587997(32)	0.0001275(47)	0.000005587(97)	0.000004629(75)
25	0.0181523(81)	0.00134699(10)	0.002098973(70)	0.000333(17)	0.00000944(22)	0.00000727(15)
44	0.087852(25)	0.00535156(18)	0.00857369(13)	0.000872(51)	0.00001465(38)	0.00001071(27)
63	0.44452(42)	0.0274458(20)	0.0471025(13)	0.00268(72)	0.0000299(34)	0.0000215(23)
70	0.87333(49)	0.0567002(18)	0.1008647(13)	0.00391(95)	0.0000358(38)	0.0000254(27)
83	3.39863(52)	0.2853917(17)	0.5542225(12)	0.0097(10)	0.0000699(35)	0.0000492(25)
92	10.5547(13)	1.1947167(36)	2.5074061(26)	0.0178(27)	0.0001037(74)	0.0000723(51)

Table 5.5: Dependence on the nuclear model for corrected potential.

Z	$\Delta\varepsilon_{el}^{pl-\text{sphere}}$	$\Delta\varepsilon_{mu}^{pl-\text{sphere}}$	$\Delta\varepsilon_{had}^{pl-\text{sphere}}$	$\Delta\varepsilon_{el}^{\text{fermi-sphere}}$	$\Delta\varepsilon_{mu}^{\text{fermi-sphere}}$	$\Delta\varepsilon_{had}^{\text{fermi-sphere}}$
1	0.0001324(12)	0.000025061(98)	0.00004546(11)			
2	0.00045296(62)	0.000062091(28)	0.000103127(24)			
4	0.0012704(49)	0.00013737(13)	0.0002180161(99)	0.000060(23)	0.00000353(31)	0.00000315(63)
5	0.001549(26)	0.00017135(72)	0.00027304(57)	0.000079(83)	0.0000049(27)	0.0000045(26)
10	0.0038131(21)	0.000371352(43)	0.0005812039(32)	0.0001208(43)	0.000005563(97)	0.000004616(90)
25	0.0141229(64)	0.001248827(94)	0.001954194(69)	0.000275(13)	0.00000932(20)	0.00000721(15)
44	0.048661(15)	0.00423715(17)	0.00684603(12)	0.000561(30)	0.00001414(35)	0.00001046(15)
63	0.16599(18)	0.0166951(17)	0.0289589(12)	0.00127(30)	0.0000279(30)	0.0000204(21)
70	0.27967(17)	0.0302185(15)	0.0542981(11)	0.00167(35)	0.0000328(32)	0.0000237(23)
83	0.79286(15)	0.1099914(13)	0.21534723(92)	0.00328(30)	0.0000614(27)	0.0000444(19)
92	1.90527(33)	0.3360041(26)	0.7091884(18)	0.00514(66)	0.0000879(54)	0.0000631(37)

simplification might as well be very inaccurate. Similarly to the g-factor, we would also need to consider interactions between the $1s$ and $2s$ electrons and all possible combinations in which the Uehling potential might interact in such a case. Furthermore, we would also have to consider all the possibilities in which the magnetic potential interacts with the $1s$ electrons. In case of the g-factor, these terms cancel each other out because the absolute value of the energy shift for the spin up and spin down electron is the same. However, for hyperfine splitting, that is not the case, leading to five additional Feynman diagrams that have to be considered arising from the different places the Uehling potential can interact.

Table 5.6: Electronic vacuum polarisation corrections for $2s$ states.

Z	$\varepsilon_{el}^{wf,pl}$	$\varepsilon_{el}^{pot,pl}$	$\varepsilon_{el,\mathrm{sphere}}^{wf,fns}$	$\varepsilon_{el,\mathrm{fermi}}^{wf,fns}$	$\varepsilon_{el,\mathrm{sphere}}^{pot,fns}$	$\varepsilon_{el,\mathrm{fermi}}^{pot,fns}$
1	0.0087480	0.00856350	0.0086153(11)		0.0084312(11)	
2	0.01773110	0.01707253	0.01727519(63)		0.01661945(62)	
4	0.0363164	0.0339916	0.0350248(50)	0.0350848(54)	0.0327203(49)	0.0327802(27)
5	0.045914	0.042430	0.044330(26)	0.044101(28)	0.040880(56)	0.040959(28)
10	0.0972437	0.0849339	0.0931777(23)	0.0933049(24)	0.0811029(21)	0.0812243(23)
25	0.3024963	0.2282650	0.2838533(83)	0.2841949(86)	0.2137208(66)	0.2140035(68)
44	0.824157	0.508624	0.728278(28)	0.729229(28)	0.455278(16)	0.455892(17)
63	2.35860	1.11359	1.82183(51)	1.82506(35)	0.91259(21)	0.91413(15)
70	3.70526	1.54155	2.59865(58)	2.60361(59)	1.18673(21)	1.18884(21)
83	10.18887	3.14582	5.39983(73)	5.41345(75)	2.03183(21)	2.03643(22)
92	25.5485	5.94539	9.3306(20)	9.3579(21)	3.03565(49)	3.04347(50)

Table 5.7: Muonic vacuum polarisation corrections for $2s$ states.

Z	$\varepsilon_{mu}^{wf,pl}$	$\varepsilon_{mu}^{pot,pl}$	$\varepsilon_{mu,\mathrm{sphere}}^{wf,fns}$	$\varepsilon_{mu,\mathrm{fermi}}^{wf,fns}$	$\varepsilon_{mu,\mathrm{sphere}}^{pot,fns}$	$\varepsilon_{mu,\mathrm{fermi}}^{pot,fns}$
1	0.000041619	0.000041606	0.000016552(96)		0.000016440(81)	
2	0.000083440	0.000083375	0.000021300(28)		0.000021273(28)	
4	0.00016839	0.00016799	0.00003062(13)	0.00003415(18)	0.00003051(13)	0.00003404(17)
5	0.00021185	0.00021111	0.00003972(72)	0.00004464(97)	0.00003956(72)	0.0000445(10)
10	0.000446079	0.000440673	0.000068249(44)	0.000073853(55)	0.000067575(43)	0.000073164(54)
25	0.00156307	0.001455928	0.00017587(10)	0.00018558(12)	0.000169803(98)	0.00017940(12)
44	0.00628753	0.00503132	0.00042069(20)	0.00043675(22)	0.00038607(18)	0.00040158(20)
63	0.0343610	0.0211769	0.0011307(24)	0.0011669(18)	0.0009641(21)	0.0009979(43)
70	0.0735303	0.0396513	0.0016097(23)	0.0016551(25)	0.0013255(19)	0.0013671(21)
83	0.4044851	0.1572363	0.0036796(24)	0.0037776(25)	0.0028103(18)	0.0028964(20)
92	1.8299643	0.5173064	0.0065634(55)	0.0067213(59)	0.0047049(40)	0.0048385(43)

Table 5.8: Hadronic vacuum polarisation corrections for $2s$ states.

Z	$\varepsilon_{had}^{wf,pl}$	$\varepsilon_{had}^{pot,pl}$	$\varepsilon_{had,\mathrm{sphere}}^{wf,fns}$	$\varepsilon_{had,\mathrm{fermi}}^{wf,fns}$	$\varepsilon_{had,\mathrm{sphere}}^{pot,fns}$	$\varepsilon_{had,\mathrm{fermi}}^{pot,fns}$
1	0.00005931	0.00005930	0.00001385(11)		0.00001384(11)	
2	0.000118921	0.000118850	0.000015721(25)		0.000015704(25)	
4	0.00024007	0.00023958	0.00002147(10)	0.00002464(15)	0.00002140(10)	0.00002457(15)
5	0.00030213	0.00030120	0.00002795(57)	0.00003245(83)	0.00002785(57)	0.00003234(84)
10	0.000637911	0.000630653	0.000047148(32)	0.000051793(43)	0.000046716(32)	0.000051353(42)
25	0.002281580	0.002128635	0.000119937(72)	0.000127417(86)	0.000116077(70)	0.000123497(85)
44	0.00968381	0.00776779	0.00028454(14)	0.00029629(15)	0.00026240(13)	0.00027386(14)
63	0.0577908	0.0357159	0.0007625(17)	0.0007885(12)	0.0006554(15)	0.0006801(11)
70	0.1290163	0.0697652	0.0010836(16)	0.0011158(17)	0.0009001(14)	0.0009302(15)
83	0.7807174	0.3042536	0.0024752(16)	0.0025442(17)	0.0019118(13)	0.0019740(14)
92	3.8305248	1.0851223	0.0044098(38)	0.0045200(40)	0.0032003(28)	0.0032962(30)

6 Summary and Outlook

In this thesis, we investigate QED effects on the bound electron in the presence of hyperfine splitting. In particular, we have calculate the effect of leptonic and hadronic vacuum polarisation on the energy level of a $1s$ and $2s$ electron bound to a nucleus generating a magnetic field.

In chapters 2 and 3, we present the theoretical framework necessary for this thesis. In chapter 2, we introduce the Dirac equation and discuss how a finite nucleus influences the resulting wave functions. We discuss how QED effects need to be treated in the framework of a bound electron and introduce the perturbative expressions used to determine our results. We explain the effect of hyperfine splitting and introduce the convention used to parameterise the shift in energy when considering the previously mentioned QED corrections. In chapter 3, we explain both leptonic and hadronic vacuum polarisation in more detail and introduce the Uehling potential as the perturbative potential acting on the energy level. For hadronic VP, we introduce a semi-empirical approach, allowing us to get an expression of the polarisation tensor without the difficulties a QCD approach would entail.

In chapter 4, we introduce the numerical methods used to calculate the QED corrections. We motivate the use of splines due to their computational simplicity and easy way to be implemented and controled. In particular, we consider the use of B-splines over splines such as the Bézier spline by showing that they meet the criteria necessary to describe the radial wave functions since they are C^2 continuous. Using a finite basis set approach to the Dirac equation, we link B-splines to the perturbative expressions that are used to determine our results.

In chapter 5, we distinguish between the two possibilities in which the magnetic potential and the Uehling potential could act on the wave function at second order and derive the specific expressions for the convention introduced in chapter 2. This results in

$$\varepsilon^{\text{wf,fns}} = -\frac{\pi}{\alpha}\frac{\int dr V_{\text{Ueh}}(r)\left(G_{n\kappa}(r)X_{\text{mag}}(r) + F_{n\kappa}(r)Y_{\text{mag}}(r)\right)}{m_e^2(Z\alpha)^3}, \tag{6.1}$$

$$\varepsilon^{\text{wf,pl}} = -\frac{\pi}{\alpha}\frac{\int dr V_{\text{Ueh}}(r)\left(G_{n\kappa}(r)X_{\text{mag}}(r) + F_{n\kappa}(r)Y_{\text{mag}}(r)\right)}{m_e^2(Z\alpha)^3} \tag{6.2}$$

for the correction to the wave function and

$$\varepsilon^{\text{pot,fns}} = \frac{\pi}{\alpha}\frac{\int dr \frac{1}{r^2} G_{n\kappa}(r)F_{n\kappa}(r)F_{\text{ML}}(r)}{m_e^2(Z\alpha)^3} \tag{6.3}$$

for the correction to the magnetic potential.
These expressions are evaluated using the numerical methods discussed in chapter 4 for multiple nuclei. The results coincide well within literature values, as well as with the approximate formulas for small, point-like nuclei. They show that the effect of both leptonic and hadronic VP is greater than the uncertainty of the radius, making them relevant for future measurements. However, as mentioned before, the nuclear model considerably changes the results. It is, therefore, necessary to understand the nucleus better in order to be able to perform high-precision experiments for hyperfine splitting. In turn, this also means that we might be able to further our understanding of the nucleus by studying hyperfine structure. Assuming the nucleus to follow the Fermi model, it might, at some point, be possible to use experimental data of the energy shift to determine more accurate descriptions for the nuclear parameters.

Following this work, there are many future calculations that can be done. Firstly, in addition to the calculations for $2s$ electrons, one can also consider the interactions that would take place in lithium- and boron-like ions. It would be interesting to consider how the nuclear model impacts the energy level of the $2s$ electron in that case. These results could also be used to determine the fine-structure constant when compared to hydrogen-like ions. Furthermore, it might be possible to find a new expression for the Uehing potential of hadronic VP using only QCD. Repeating these calculations with the new Uehling potential might lead to different results, which would indicate an interesting discrepancy.

A List of isotopes used

Table A.1: Isotopes and their radii [29]

Nuclear charge Z	Mass number A	R_{rms}(fm)	ΔR(fm)
1	1	0.8783	0.0086
2	4	1.6755	0.0028
4	9	2.5190	0.0120
5	10	2.4277	0.0499
10	20	3.0055	0.0021
25	55	3.7057	0.0022
44	104	4.5098	0.0020
63	145	4.9663	0.0091
70	176	5.3215	0.0062
83	209	5.5211	0.0026
92	238	5.8571	0.0033

B Virial relations for the Dirac equation

A different way to write the magnetically perturbated wave function in Eq. (5.5) is to write it as

$$\sum_{\substack{n' \\ n \neq n'}} \frac{|\psi_{n'\kappa}\rangle\langle\psi_{n'\kappa}|\sigma_1/r^2|\psi_{n\kappa}\rangle}{E_{n\kappa} - E_{n'\kappa}}. \tag{B.1}$$

Following Ref. [25], we want to evaluate this expression using the virial theorem. For a non-relativistic particle moving in a central field $V(r)$, the theorem relates the average value of the kinetic energy $\langle T\rangle$ to the field with the equation

$$\langle T\rangle = \frac{1}{2}\langle r\frac{dV}{dr}\rangle. \tag{B.2}$$

For a relativistic particle moving in a central field $V(r)$, the theorem states

$$E = \langle m\beta\rangle + \langle r\frac{dV}{dr}\rangle + \langle V\rangle \tag{B.3}$$

where E denotes the bound state energy. In case of the Coulomb field, this is simplified to

$$E = \langle m\beta\rangle. \tag{B.4}$$

Using the notation introduced in Eq. (B.1), we can write the Hamiltonian as

$$H_\kappa = -i\sigma_2\frac{d}{dr} + \frac{\kappa}{r}\sigma_1 + m\sigma_3 + V\mathbb{1}. \tag{B.5}$$

With the eigenvalues $E_{n\kappa}$ and taking into account the self-adjointness of H_κ, we can write the equations

$$\langle n'\kappa|(H_\kappa Q - QH_\kappa|n\kappa\rangle = (E_{n'\kappa} - E_{n\kappa})\langle n'\kappa|Q|n\kappa\rangle \tag{B.6}$$
$$\langle n'\kappa|(H_\kappa Q + QH_\kappa|n\kappa\rangle = (E_{n'\kappa} + E_{n\kappa})\langle n'\kappa|Q|n\kappa\rangle \tag{B.7}$$

with $Q = r^s, i\sigma_2 r^s, \sigma_3 r^s, \sigma_1 r^s$ and an integer s.
We can apply these equations to average values of physical quantities, i.e. using the

Hellmann-Feynman theorem

$$\frac{\partial E_{n\kappa}}{\partial \kappa} = \langle \psi_{n\kappa} | \frac{\partial H_\kappa}{\partial \kappa} | \psi_{n\kappa} \rangle = \langle \psi_{n\kappa} | \frac{\sigma_1}{r} | \psi_{n\kappa} \rangle. \tag{B.8}$$

After some calculations, we then arrive at the expressions

$$\begin{aligned} X_{mag} = \frac{1}{a^2+b} \Bigg(& \frac{a}{r} F(r) + \frac{2a\kappa}{r} F(r) + \frac{b}{r} G(r) - \frac{b}{\kappa} F(r)(E_{Som} + m) \\ & - \frac{a^3 \kappa m}{4N^3 \gamma} G(r) \Bigg) - \frac{a\left(2E_{Som} - \frac{m}{\kappa}\right)}{a^2+b} \tilde{G}(r) \end{aligned} \tag{B.9}$$

$$\begin{aligned} Y_{mag} = \frac{1}{a^2+b} \Bigg(& \frac{a}{r} G(r) - \frac{2a\kappa}{r} G(r) - \frac{b}{r} F(r) - \frac{b}{\kappa} G(r)(-E_{Som} + m) \\ & - \frac{a^3 \kappa m}{4N^3 \gamma} F(r) \Bigg) - \frac{a\left(2E_{Som} - \frac{m}{\kappa}\right)}{a^2+b} \tilde{F}(r) \end{aligned} \tag{B.10}$$

(B.11)

with γ as defined in Eq. (2.15), the unperturbated energy for point-like nuclei E_{Som} defined in Eq. (2.17) and

$$N = \sqrt{(\gamma + n - |\kappa|)^2 + (Z\alpha)^2}, \quad a = 2Z\alpha, \quad b = 1 - 4\kappa^2. \tag{B.12}$$

Following are formulas in case of point-like nuclei for the expression [25]

$$\frac{\partial}{\partial \kappa} |n\kappa\rangle = \begin{pmatrix} \tilde{G}_{ns}(r) \\ \tilde{F}_{ns}(r) \end{pmatrix} \tag{B.13}$$

for 1s states

$$\tilde{G}_{1s}(r) = \frac{k}{\sqrt{1-\gamma}} e^{-\frac{t}{2}} t^\gamma \left(\frac{\psi(2\gamma+1)}{\gamma} + \gamma + 1 - \frac{1}{2\gamma} - \frac{t}{2} - \frac{\ln t}{\gamma} \right) \tag{B.14}$$

$$\tilde{F}_{1s}(r) = -\frac{k}{\sqrt{1+\gamma}} e^{-\frac{t}{2}} t^\gamma \left(\frac{\psi(2\gamma+1)}{\gamma} + \gamma + 1 + \frac{1}{2\gamma} - \frac{t}{2} - \frac{\ln t}{\gamma} \right) \tag{B.15}$$

with the derivative $\psi(x) = \frac{d}{dx} \ln \Gamma(x)$, the gamma-function $\Gamma(x)$ and

$$t = \frac{2\alpha Z m r}{N}, \quad k = \frac{(2\alpha Z)^{\frac{2}{3}} m^{\frac{1}{2}}}{2\sqrt{2\Gamma(2\gamma+1)}} \tag{B.16}$$

and for 2s states

$$\begin{aligned}\tilde{G}_{2s}(r) = k' e^{-\frac{t}{2}} t^{\gamma} \frac{\sqrt{2+N}}{N^2-2} \Bigg[& \frac{t^2}{2(N-1)} \\ & - \left(\frac{2N^4 - 4N^3 + 5N^2 - 3N + 2}{2N(N-1)^2} + \frac{2\psi(2\gamma+1)}{N-1} \right) t \\ & + \frac{N^4 - 2N^3 + N - 2}{2(N-1)} + 2N\psi(2\gamma+1) + \frac{2}{N-1} t \ln t - 2N \ln t \Bigg] \end{aligned} \tag{B.17}$$

$$\begin{aligned}\tilde{F}_{2s}(r) = - k' e^{-\frac{t}{2}} t^{\gamma} \frac{\sqrt{2-N}}{N^2-2} \Bigg[& \frac{t^2}{2(N-1)} \\ & - \left(\frac{2N^4 - 2N^3 + N^2 + 3N - 2}{2N(N-1)^2} + \frac{2\psi(2\gamma+1)}{N-1} \right) t \\ & + \frac{N^5 + 5N^2 - 8N - 4}{2N(N-1)} + 2(N+2)\psi(2\gamma+1) \\ & + \frac{2}{N-1} t \ln t - 2(N+2) \ln t \Bigg] \end{aligned} \tag{B.18}$$

$$k' = \frac{\sqrt{\Gamma(2\gamma+2)}}{\Gamma(2\gamma+1)} \frac{1}{\sqrt{8N(N+1)}} \left(\frac{2\alpha Z m}{N} \right)^{\frac{1}{2}}.$$

List of Tables

Bibliography

[1] W. Greiner. *Relativistische Quantenmechanik*. Harri, 1981. ISBN 3-87144-274-7.

[2] Michael E. Peskin and Daniel V. Schroeder. *An Introduction to Quantum Field Theory*. Westview Press, 1995. ISBN 0-201-50397-2.

[3] A. Schneider, B. Sikora, S. Dickopf, M. Müller, N. S. Oreshkina, A. Rischka, I. A. Valuev, S. Ulmer, J. Walz, Z. Harman, C. H. Keitel, A. Mooser, and K. Blaum. Direct measurement of the 3He+ magnetic moments. *Nature*, 606: 878–883, 2022. doi: 10.1038/s41586-022-04761-7.

[4] P. Kusch and H. M. Foley. Precision Measurement of the Ratio of the Atomic 'g Values' in the ${}^2P_{\frac{3}{2}}$ and ${}^2P_{\frac{1}{2}}$ states of gallium. *Phys. Rev.*, 72:1256–1257, Dec 1947. doi: 10.1103/PhysRev.72.1256.2.

[5] W. Greiner and J. Reinhardt. *Quantenelektrodynamik*. Harri, 1984. ISBN 3-8171-1426-5.

[6] S. Breidenbach, E. Dizer, H. Cakir, and Z. Harman. Hadronic vacuum polarization correction to atomic energy levels. *Phys. Rev. A*, 106:042805, Oct 2022. doi: 10.1103/PhysRevA.106.042805.

[7] E. Tiesinga, P. J. Mohr, D. B. Newell, and B. N. Taylor. Codata recommended values of the fundamental physical constants: 2018. *Rev. Mod. Phys.*, 93:025010, Jun 2021. doi: 10.1103/RevModPhys.93.025010.

[8] W. Demtröder. *Atoms, Molecules and Photons*. Springer, 2018. doi: https://doi.org/10.1007/978-3-662-55523-1.

[9] A. Patoary and N. Oreshkina. Finite Nuclear Size Effect to the Fine Structure of Heavy Muonic Atoms. *The European Physical Journal D*, 72, 11 2017. doi: 10.1140/epjd/e2018-80545-9.

[10] T. Beier. The gj factor of a bound electron and the hyperfine structure splitting in hydrogenlike ions. *Physics Reports*, 339(2):79–213, 2000. ISSN 0370-1573. doi: https://doi.org/10.1016/S0370-1573(00)00071-5.

[11] F. A. Parpia and A. K. Mohanty. Relativistic basis-set calculations for atoms with fermi nuclei. *Phys. Rev. A*, 46:3735–3745, Oct 1992. doi: 10.1103/PhysRevA.46.3735.

[12] S. Weinberg. *The Quantum Theory of Fields*, volume 1. Cambridge University Press, 1995. doi: 10.1017/CBO9781139644167.

[13] W. H. Furry. On Bound States and Scattering in Positron Theory. *Phys. Rev.*, 81:115–124, Jan 1951. doi: 10.1103/PhysRev.81.115.

[14] B. M. Shabaev and D. A. Telnov. Relativistic Theory of Hyperfine Structure Energy Levels for Hydrogen-Like Atoms. Educational and Methodological Manual, 1999.

[15] P. Pyykkö, E. Pajanne, and M. Inokuti. Hydrogen-like relativistic corrections for electric and magnetic hyperfine integrals. *International Journal of Quantum Chemistry*, 7(4):785–806, 1973. doi: https://doi.org/10.1002/qua.560070415.

[16] S. G. Karshenboim, V. G. Ivanov, and V. M. Shabaev. Vacuum polarization in a hydrogen-like relativistic atom: g factor of a bound electron. *Journal of Experimental and Theoretical Physics*, 93:477–484, 09 2001. doi: 10.1134/1.1410592.

[17] J. S. Breidenbach. Hadronic vacuum polarization in atoms. Bachelor's thesis, Ruprecht Karl University of Heidelberg, Heidelberg, Germany, 2018.

[18] R. G. Newton. Optical theorem and beyond. *American Journal of Physics*, 44 (7):639–642, 07 1976. ISSN 0002-9505. doi: 10.1119/1.10324.

[19] H. Burkhardt, F. Jegerlehner, G. Penso, and C. Verzegnassi. Uncertainties in the hadronic contribution to the qed vacuum polarization. *Phys. Rev. C: Part. Fields*, 43:497, 1989. doi: 10.1007/BF01506546.

[20] H. Burkhardt and B. Pietrzyk. Update of the hadronic contribution to the qed vacuum polarization. *Physics Letters B*, 513(1):46–52, 2001. ISSN 0370-2693. doi: https://doi.org/10.1016/S0370-2693(01)00393-8.

[21] The MathWorks Inc. Matlab version: 8.4.0 (R2014b), 2014.

[22] V. M. Shabaev, I. I. Tupitsyn, V. A. Yerokhin, G. Plunien, and G. Soff. Dual Kinetic Balance Approach to Basis-Set Expansions for the Dirac Equation. *Phys. Rev. Lett.*, 93:130405, Sep 2004. doi: 10.1103/PhysRevLett.93.130405.

[23] W. R. Johnson, S. A. Blundell, and J. Sapirstein. Finite basis sets for the Dirac equation constructed from b splines. *Physical review. A, General physics*, 37 (2):307—315, January 1988. ISSN 0556-2791. doi: 10.1103/physreva.37.307.

[24] H. Cakir. *Quantum Electrodynamic Theory of Few-Electron Highly Charged Ions*. PhD thesis, Ruprecht Karl University of Heidelberg, Heidelberg, Germany, 2020.

[25] Vladimir M. Shabaev. *Virial Relations for the Dirac Equation and Their Applications to Calculations of Hydrogen-Like Atoms*, pages 97–113. Springer Berlin Heidelberg, Berlin, Heidelberg, 2003. ISBN 978-3-540-45059-7. doi: 10.1007/978-3-540-45059-7_6.

[26] S. M. Schneider, W. Greiner, and G. Soff. Vacuum-polarization contribution to the hyperfine-structure splitting of hydrogenlike atoms. *Phys. Rev. A*, 50: 118–122, Jul 1994. doi: 10.1103/PhysRevA.50.118.

[27] S. G. Karshenboim, V. G. Ivanov, and V. M. Shabaev. Polarization of vacuum in a hydrogen-like relativistic atom: Hyperfine structure. *Journal of Experimental and Theoretical Physics*, 90:59–65, 2000. doi: https://doi.org/10.1134/1.559094.

[28] H. Cakir, N. S. Oreshkina, I. A. Valuev, V. Debierre, V. A. Yerokhin, C. H. Keitel, and Z. Harman. Improved access to the fine-structure constant with the simplest atomic systems, 2020.

[29] I. Angeli and K.P. Marinova. Table of experimental nuclear ground state charge radii: An update. *Atomic Data and Nuclear Data Tables*, 99(1):69–95, 2013. ISSN 0092-640X. doi: https://doi.org/10.1016/j.adt.2011.12.006.

Acknowledgements

I would like to thank the following people for their help over the course of this thesis:

- Bastian Sikora, for his incredible help throughout this thesis. His insight and the multiple conversations we had helped to greatly further both the results as well as my personal understanding of the topic.

- Zoltán Harman, my supervisor, who was always available and happy to assist when questions arose. Furthermore, his lecture on QED was a remarkably comprehensible introduction to this field of study.

- Halil Cakir, for taking his time to answer my questions on the code.

- The people at the Max Planck Institute, for their warm welcome.

- Maris Bruckmann, who had to battle through all my punctuation errors without giving up whilst proofreading this thesis.

Declaration of Authorship

Ich versichere, dass ich diese Arbeit selbstständig verfasst habe und keine anderen als die angegebenen Quellen und Hilfsmittel benutzt habe.

I hereby certify that this thesis was composed by myself and that I did not use other resources than those listed.

Heidelberg, den 24.11.2023 .....